

## Article

# A Low-Density Polyethylene-Reinforced Ternary Phase-Change Composite with High Thermal Conductivity for Battery Thermal Management

Yueliang Yu <sup>1,†</sup>, Hongmei Qin <sup>1,†</sup>, Shusen Ran <sup>1</sup>, Jinhui Song <sup>1</sup>, Wenlai Xia <sup>1</sup>, Shan Wang <sup>1,2,\*</sup>   
and Chuanxi Xiong <sup>1,2,\*</sup>

<sup>1</sup> School of Materials Science and Engineering, Wuhan University of Technology, Wuhan 430070, China

<sup>2</sup> Hubei Engineering Research Center for Green Precision Material Forming, Wuhan 430070, China

\* Correspondence: shanwang@whut.edu.cn (S.W.); cxiong@whut.edu.cn (C.X.)

† These authors contributed equally to this work.

**Abstract:** Paraffin phase change materials (PCMs) exhibit great potential in battery thermal management (BTM); nevertheless, their application has been hampered by the handicap of low thermal conductivity, leakage, and volume expansion during phase transition. In this work, ternary composite PCMs formed of paraffin, expanded graphite (EG), and low-density polyethylene (LDPE) were developed for application in BTM. The structure and properties of the composite PCMs were characterized via X-ray diffraction, scanning electron microscopy, differential scanning calorimetry, and thermal constant analysis. The result shows that EG can form a large-size graphite frame as heat conduction paths to improve the thermal conductivity of the composite PCM, and LDPE can form an interpenetrating network within the composite PCM to resist the internal stress of paraffin expansion and prevent deformation. The latent heat and thermal conductivity of the composite PCMs loaded with 10 wt% EG and 4 wt% LDPE can reach 172.06 J/g and 3.85 Wm<sup>-1</sup>K<sup>-1</sup> with a relatively low leakage ratio of 6.2 wt%. Remarkably, the composite PCMs could reduce the temperature rise of the battery by 55.1%. In brief, this work provides a feasible route to develop high-performance PCMs for BTM.

**Keywords:** phase change material; paraffin; expanded graphite; low-density polyethylene; thermal conductivity; battery thermal management



**Citation:** Yu, Y.; Qin, H.; Ran, S.; Song, J.; Xia, W.; Wang, S.; Xiong, C. A Low-Density Polyethylene-Reinforced Ternary Phase-Change Composite with High Thermal Conductivity for Battery Thermal Management. *Energies* **2023**, *16*, 3838. <https://doi.org/10.3390/en16093838>

Academic Editor: Antonino S. Arico

Received: 23 March 2023

Revised: 16 April 2023

Accepted: 27 April 2023

Published: 29 April 2023



**Copyright:** © 2023 by the authors. Licensee MDPI, Basel, Switzerland. This article is an open access article distributed under the terms and conditions of the Creative Commons Attribution (CC BY) license (<https://creativecommons.org/licenses/by/4.0/>).

## 1. Introduction

Following the successful commercialization of electric vehicles, the thermal management of Li-ion power battery pack, the core component of an electric vehicle, has received extensive attention [1]. During operation, the battery will inevitably generate reaction heat, polarization heat, and Joule heat [2]. Due to the limited space in the vehicles, these batteries are stacked closely, and such a situation poses a significant challenge for heat dissipation [3]. The high-temperature operation will accelerate the ageing of the battery and reduce its capacity [4]. Ramadass et al. [5] reported that the capacity of Li-ion batteries decreased by 60% after 800 times discharges at 50 °C, and by 70% after 600 times discharges at 55 °C. Chester et al. [6] tested the service performance of lithium batteries at 30–40 °C and found that the calendar life of the batteries was reduced by 2 months for every 1 °C increase in temperature. Therefore, it is very important to develop an efficient battery thermal management (BTM) system.

At present, the BTM systems mainly include air cooling, liquid cooling, and phase change material (PCM) cooling [7]. However, the heat dissipation effect of air cooling is unsatisfactory due to the low specific heat capacity and low thermal conductivity of air [8]. In addition, liquid cooling is costly and less safe, with the risk of leakage causing short circuits in the battery packs [9]. In contrast, the BTM system based on PCMs has attracted

much attention because of the advantages of safety, low cost, and high efficiency [10]. In addition, it is a passive BTM system that does not require fans or pumps to drive fluid movement without additional energy consumption [11].

The heat energy absorbed by PCMs can be divided into sensible heat and latent heat. The former is related to the specific heat capacity and temperature rise and has a low heat storage density [12], while the latter is related to the enthalpy of phase change, and its heat storage density is high [13]. In the phase-change BTM system, a small fraction of the battery heat is initially absorbed as sensible heat, and then most of it is absorbed as latent heat when the temperature reaches the phase-change temperature of the material, during which time the battery temperature can be regulated, since the phase transition process of the substance takes place at approximately constant temperature [14]. Among the investigated PCMs, paraffin is the most suitable for BTM applications [15]. The main component of paraffin is *n*-alkane with the general chemical formula  $C_nH_{2n+2}$ , whose latent heat is over 200 J/g, and melting point increases with the increase of the number of carbon atoms, varying from  $-30\text{ }^\circ\text{C}$  to  $95\text{ }^\circ\text{C}$  [16]. Paraffin is derived from fossil fuels, such as petroleum, coal, and shale oil, and is a by-product of the petrochemical industry, which has the advantage of the abundance and low cost [17]. Moreover, paraffin is chemically stable, non-toxic, non-corrosive, non-flammable, and non-explosive, ensuring its safety and harmlessness for the surroundings [18]. However, comparable to other PCMs, paraffin also suffers from leakage during phase transition, preventing it from being applied directly in BTM alone [19]. Moreover, the thermal conductivity of paraffin is too low to absorb the battery heat in time [20].

A common strategy to suppress paraffin leakage and improve its thermal conductivity is to incorporate other functional materials into the paraffin to make composite PCMs [21]. At present, various porous media based on thermally conductive materials, such as metal foam, porous ceramics, and expanded graphite (EG), have been developed to encapsulate paraffin [22]. Such materials can not only achieve a high loading fraction of paraffin but also directly act as a continuous heat-conducting network to improve the thermal conductivity of the composite PCM [23]. Among them, EG is preferred because of its low density, low cost, high corrosion resistance, and good compatibility with organic PCMs [24]. EG is a high-porosity powder material obtained by oxidation, intercalation, and high-temperature expansion of natural flake graphite [25]. In addition, EG can adsorb paraffin by capillary force, in which the loading fraction of paraffin can reach 85.6 wt% [26]. By compression induction, the EG powder is connected by van der Waals forces and can be used as a block [27]. However, the EG block formed by such a weak bonding force may not resist the internal stress of paraffin expansion. Lv et al. [28] reported the cracking phenomenon of EG/paraffin composite when applied to BTM. The volume of paraffin can expand by 12.36% after melting [29], which will undoubtedly cause significant volume contraction and cracking in the matrix [30]. Such undesirable deformation may introduce an air gap between the composite PCM and the battery surface, which will reduce the heat dissipation efficiency of the phase-change BTM system. To address this problem, Li et al. [3] prepared a layer of inorganic  $\text{SiO}_2$  coating on the surface of the EG/paraffin composite via a sol-gel process to improve its mechanical strength. However, this method requires a long reaction time and a large amount of water medium, associated with water pollution problems and complicated post-treatment processes [31].

In this work, a simple strategy for solving the cracking phenomenon of the EG/paraffin composite is presented. Low-density polyethylene (LDPE) was selected as the reinforcing material to strengthen the EG/paraffin composite. Through simple physical blending and cold pressing, an LDPE-reinforced ternary composite PCM was developed. The amount of LDPE is kept to a minimum to ensure that the latent heat of the composite PCM is as high as possible. The results show that when the mass fraction of LDPE reaches 40% of the EG, the composite PCM has sufficient mechanical strength to resist the internal stress of paraffin expansion and does not crack under heating. Significantly, when 10 wt% EG and 4 wt% LDPE are added, the composite PCM has a high thermal conductivity of  $3.85\text{ W m}^{-1}\text{ K}^{-1}$

and a high latent heat of 172.06 J/g and shows the best thermal management performance, reducing the temperature rise of the battery by 55.1%.

## 2. Materials and Methods

### 2.1. Materials

Paraffin with a melting point of 42 °C was supplied by Shanghai Joule Wax Co., Ltd. (Shanghai, China). Expanded graphite (EG, SYH-800) with an initial expansion volume of 600 mL/g was purchased from Qingdao Yanhai Carbon Materials Co., Ltd. (Qingdao, China). Low-density polyethylene (LDPE, LD163, Sinopec Beijing Yanshan Petrochemical Co., Ltd., Beijing, China) with a melt flow index (MFI) of 0.39 g/10 min was selected as the reinforcing material. All the materials were used as received without further purification.

### 2.2. Preparation of EG/LDPE/Paraffin Composites

The EG/LDPE/paraffin composites were prepared by a two-step process. First, the appropriate amount of paraffin and EG was placed in a beaker at 80 °C for 6 h, during which time the paraffin melted and penetrated EG pores. Then, LDPE and EG/paraffin powder were mixed at 120 °C for 10 min with a mixing speed of 20 rpm using an internal mixer (QE-70A, Wuhan Qien Science & Technology Development Co., Ltd., Wuhan, China). The obtained composite was cold-pressed into cylinders with a size of  $\Phi 30 \times 5$  mm at 20 MPa. The compositions of the prepared samples are summarized in Table 1.

**Table 1.** The compositions of different composite PCMs.

Sample	Paraffin (g)	EG (g)	LDPE (g)
S-1	90	10	0
PCM-1	93	5	2
PCM-2	86	10	4
PCM-3	79	15	6
PCM-4	72	20	8

### 2.3. Characterization of Composite PCMs

The cross-sectional morphologies of the composite PCMs were observed with a field-emission scanning electron microscope (SEM, Zeiss Ultra Plus, Carl Zeiss AG, Oberkochen, Germany) operating at an accelerating voltage of 5 kV. The Fourier-transform infrared (FTIR) spectra of paraffin, LDPE, EG, and composite PCMs were measured by using a Nicolet FTIR spectrometer (Nicolet 6700, Thermo Fisher Scientific, Waltham, MA, USA) between 500 and 4000  $\text{cm}^{-1}$ . The XRD patterns of paraffin, LDPE, EG, and composite PCMs were recorded by an X-ray diffractometer (D8 Advance, Bruker Corporation, Karlsruhe, Germany) at 40 kV/40 mA with a Cu  $K\alpha$  radiation ( $\lambda = 1.54 \text{ \AA}$ ), the scanning  $2\theta$  ranged from 5° to 50°, and the speed was set to 10°  $\text{min}^{-1}$ .

The thermal conductivity of paraffin and composite PCMs was measured by a thermal constant analyzer (TPS 2500S, Hot Disk AB, Goteborg, Sweden), using the transient plane heat source method. The melting enthalpies, solidification enthalpies, and phase change temperatures of the paraffin and composite PCMs were measured by a differential scanning calorimeter (DSC 25, TA Instruments, Wilmington, NC, USA). The test temperature ranged from 0 °C to 80 °C at a heating and cooling rate of 5 °C/min. Before testing, the sample was preheated at 80 °C for 5 min and then cooled to 0 °C to eliminate the effects of thermal history. Thermal gravimetric analysis (TGA) of paraffin, LDPE, and composite PCMs was performed by a synchronous thermal analyzer (STA2500, NETZSCH Group, Selb, Germany) in the nitrogen atmosphere from room temperature to 600 °C at a heating rate of 10 °C/min.

For the leakage measurement, the samples were placed on the filter paper and then subjected to heating and cooling cycles from ambient temperature to 80 °C. The weight loss ratio ( $wl\%$ ) was calculated by Equation (1):

$$wl\% = \frac{m_0 - m_n}{m_0} \times 100\% \quad (1)$$

where  $m_0$  is the initial mass of the sample, and  $m_n$  is the mass after the cycles.

#### 2.4. Thermal Management Performance Test of Composite PCMs

A homemade experimental device was established to assess the thermal management performance of the as-prepared composite PCMs. As shown in Figure 1, the composite PCMs were molded into blocks with semicircular grooves of 18 mm diameter for storing the 18,650 lithium battery and then fixed with a layer of insulating polyimide tape. The cylindrical battery was made by stacking the positive electrode, the negative electrode, and the diaphragm into a thin film, and then through the winding process, whose heat generation is uniform everywhere [1]. Therefore, it is rational to take the temperature variations in the middle surface of the battery as an evaluation index of the thermal management performance of the composite PCMs. The temperature data were recorded by a handheld temperature tester (JK804, Shenzhen Bost Electronic Instrument Co., Ltd., Shenzhen, China) with a K-type thermocouple. Such a thermocouple works by converting the temperature signal into the electric potential signal, so it was also fixed by the insulating polyimide tape. In addition, the device was left to stand for a while before testing until it reached 25 °C.

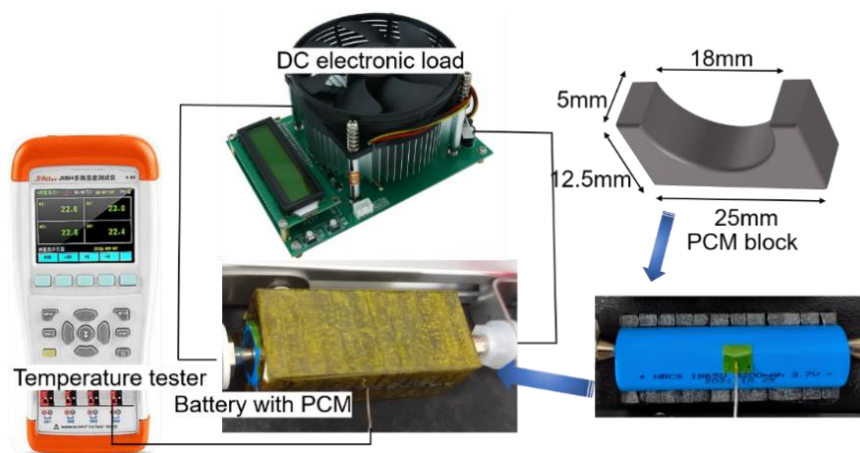


**Figure 1.** Experimental device for battery thermal management system.

The battery used in the test was commercially purchased and manufactured by BAK Power Battery (Shenzhen, China). It has a nominal capacity of 3200 mAh and its end-of-charge, nominal, and end-of-discharge voltages are 4.2, 3.7, and 2.75 V, respectively. The charging process of the battery was completed by the manufacturer's standard charger, the current was uncertain; therefore, only the temperature variations during the discharge process were recorded. The full-charge battery discharged at 1 C (3.2 A) to the cut-off voltage, with and without composite PCM. During charging and discharging, the ambient temperature was controlled at  $25 \pm 2$  °C.

### 3. Results

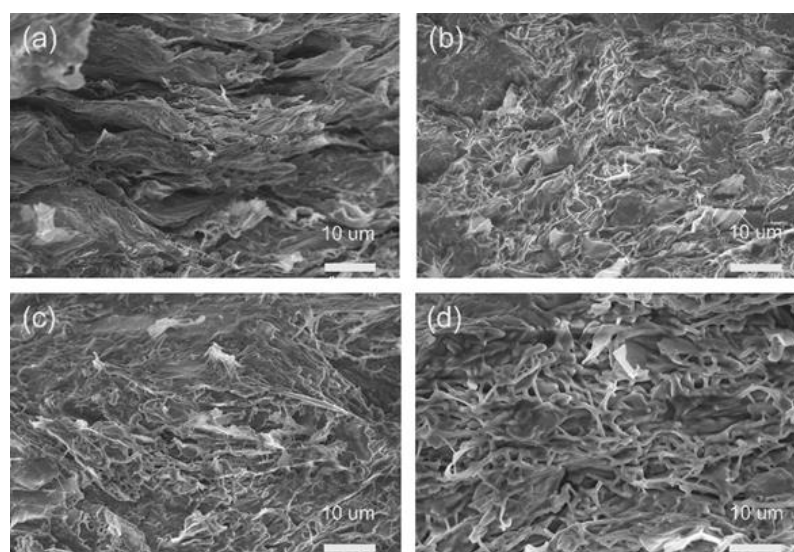
#### 3.1. Microstructural Analysis of the Composite PCMs

Figure 2 displays the preparation process and structural diagram of the composite PCMs. Firstly, the molten paraffin easily penetrated the EG pores because of its good wettability with EG [20]. Then, a large number of micron-sized graphite flakes in the EG

powder were bonded by Van der Waals forces through compression induction [14], forming a large-size graphite frame, as shown in Figure 3a. It can be used as a heat conduction path to improve the thermal conductivity of the composite PCMs. After the addition of LDPE, the filamentous polymer between the graphite sheets can be observed, as presented in Figure 3b,c. In order to determine the optimal ratio of LDPE to EG, the EG mass fractions of all the samples in Figure 3 were controlled at 10%. Until the LDPE content reached 40.0 wt% of EG, it could be observed that the LDPE formed a polymer interpenetrating network within the composite PCMs, as shown in Figure 3d. The structure may enhance the mechanical strength of composite PCMs, resisting internal stress during paraffin expansion. Here, the amount of PE is determined to be 40% of the EG mass in a composite PCM, to avoid reducing the paraffin mass fraction.



**Figure 2.** Preparation diagram of EG/paraffin composite and EG/LDPE/paraffin composite.



**Figure 3.** SEM images of (a) EG/paraffin and EG/LDPE/paraffin composites, in which the mass ratio of LDPE to EG are (b) 2:10, (c) 3:10, and (d) 4:10, respectively.

### 3.2. Chemical Composition and Crystalline Structure of the Composite PCMs

Figure 4a shows the FTIR spectra of the EG, LDPE, paraffin, and sample PCM-4. Due to the peroxide treatment, there are some polar functional groups in the EG. On the FTIR spectrum of EG, the absorption peaks at  $3447\text{ cm}^{-1}$  and  $1620\text{ cm}^{-1}$  correspond to stretching vibrations of  $-\text{OH}$  and  $-\text{NO}_2$ , respectively [32]. As for LDPE and paraffin, the absorption peaks at  $2920\text{ cm}^{-1}$  and  $2850\text{ cm}^{-1}$  are asymmetric stretching vibration and symmetric stretching vibration of  $-\text{CH}_2$ , respectively, and the absorption peak at  $1465\text{ cm}^{-1}$  and  $720\text{ cm}^{-1}$  corresponds to the  $-\text{CH}_2$  rocking vibration, while the absorption peak at  $1377\text{ cm}^{-1}$  corresponds to the  $-\text{CH}_3$  deformation vibration [33,34]. For the composite

PCM, all of the above absorption peaks can be observed in its FTIR spectrum, and no other characteristic peaks appear, indicating that no chemical reaction occurs in the mixing process. Figure 4b displays the XRD patterns of the EG, paraffin, LDPE, and sample PCM-4. There are five distinct diffraction peaks for the composite PCMs. The peak at  $26.4^\circ$  corresponds to the feature peak (0 0 2) of graphite [35]. The peaks at  $9.6^\circ$ ,  $20.7^\circ$ ,  $21.4^\circ$ , and  $23.8^\circ$  can be assigned to the diffraction of (1 1 0), (2 0 0), and other crystal planes of paraffin [36]. In addition, no new peaks appear on the XRD curve of the composite PCMs, indicating that no new phase forms, and mixing is just a physical process.

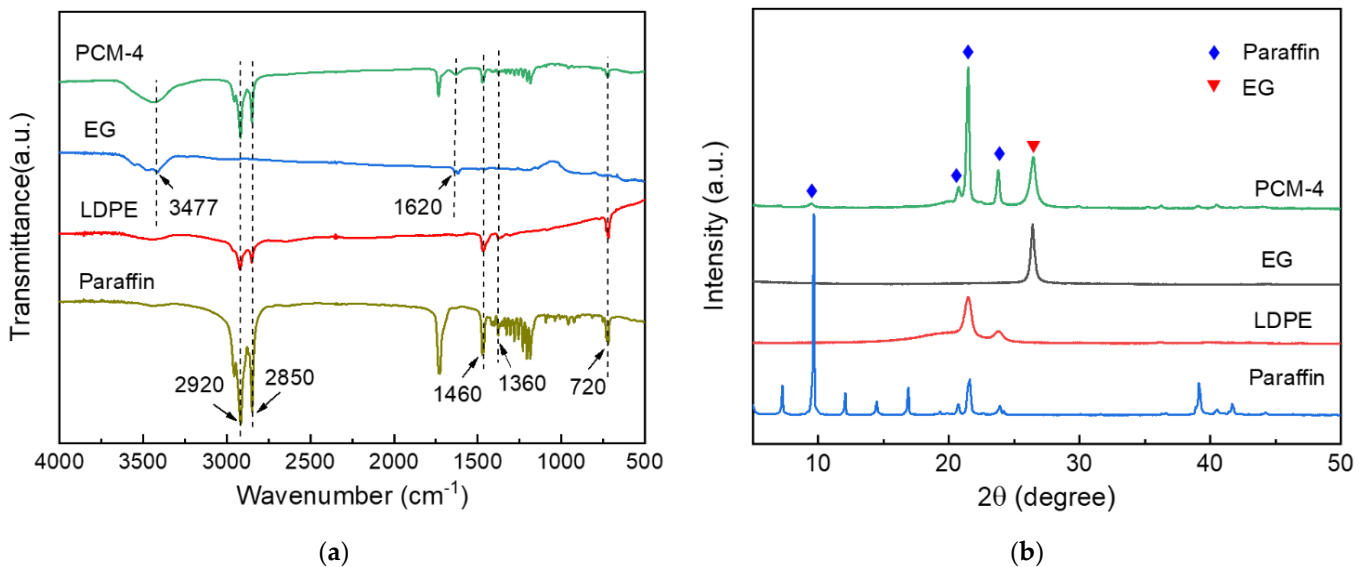


**Figure 4.** (a) FTIR spectra and (b) XRD patterns of EG, paraffin, LDPE, and PCM-4.

### 3.3. Thermal Properties of the Composite PCMs

Thermal properties, including phase change temperature, latent heat, and thermal conductivity ( $K$ ), are critical parameters of the PCMs and are quite significant to BTM. Figure 5a,b show the melting and solidification DSC curves of the paraffin and composite PCMs. Their enthalpies of melting and solidification can be obtained by integrating the area of the peak. The melting and solidification enthalpies of paraffin are 205.20 J/g and 203.89 J/g, respectively. With the decrease in paraffin mass fraction, the melting enthalpies of composite PCMs drop to 192.14 J/g, 172.06 J/g, 157.81 J/g, and 144.08 J/g, respectively, and their solidification enthalpies drop to 191.79 J/g, 170.97 J/g, 154.96 J/g, and 140.71 J/g, respectively. In terms of phase change temperature, the melting and solidification points of paraffin are  $42.79^\circ\text{C}$  and  $36.22^\circ\text{C}$ , respectively. In addition, the melting temperature range of composite PCMs is the same as that of paraffin, meaning that their operating temperature range remains unchanged. However, their solidification points drop with the decrease in paraffin mass fraction. This phenomenon can be explained based on the thermodynamic Clausius–Clapeyron equation [37], which is shown as follows:

$$\ln \frac{T_2}{T_1} = \frac{\Delta_\alpha^\beta V_m}{\Delta_\alpha^\beta H_m} (p_2 - p_1) \quad (2)$$

in which  $T_1$  and  $T_2$  are the phase change temperature in state 1 and state 2, respectively,  $\Delta_\alpha^\beta V_m$  and  $\Delta_\alpha^\beta H_m$  denote the change in volume and enthalpy during phase change from  $\alpha$ -phase to  $\beta$ -phase,  $p_1$  and  $p_2$  represent the ambient pressures in state 1 and state 2, respectively.

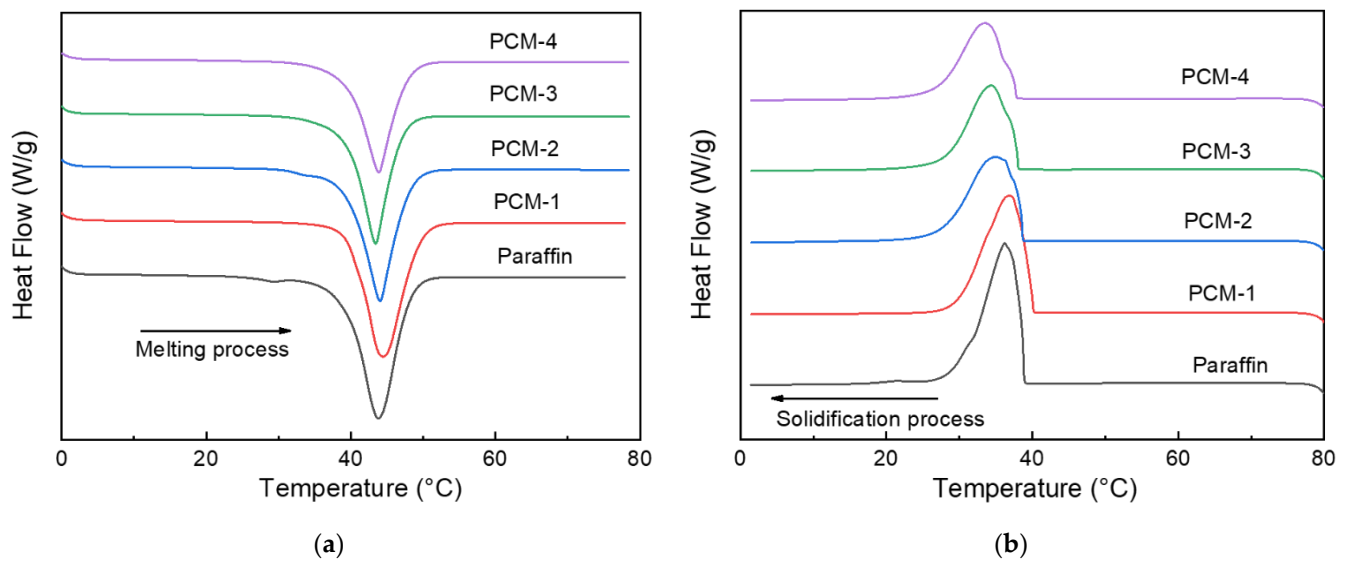


**Figure 5.** (a) Melting and (b) solidification DSC curves of paraffin and composite PCMs.

During the melting or solidification process, the enthalpy and volume of the system increase or decrease simultaneously, so the value of  $\Delta_{\alpha}^{\beta} V_m / \Delta_{\alpha}^{\beta} H_m$  is always positive. When paraffin melts and expands in volume, excess paraffin can overflow from the EG medium, and the atmospheric pressure remains unchanged ( $p_2 = p_1$ ). However, during the solidification process, the outer paraffin solidifies first to form a shell, then the contraction of the inner paraffin causes the atmospheric pressure to decrease ( $p_2 < p_1$ ). Therefore, the solidification points of the composite PCMs shift to a lower temperature.

The  $K$  of paraffin and composite PCMs are shown in Figure 6. The  $K$  of the paraffin is as low as  $0.21 \text{ Wm}^{-1}\text{K}^{-1}$ , which limits its heat storage rate, in turn preventing the timely transfer of the battery heat. Encouragingly, EG can promote heat transfer in composite PCMs due to its high thermal conductivity ( $200 \text{ Wm}^{-1}\text{K}^{-1}$ ) [38]. With the incorporation of EG, the  $K$  of composite PCMs increases rapidly. When the EG content is 5 wt%, 10 wt%, and 15 wt%, the  $K$  reaches  $2.09 \text{ Wm}^{-1}\text{K}^{-1}$ ,  $3.85 \text{ Wm}^{-1}\text{K}^{-1}$ , and  $5.39 \text{ Wm}^{-1}\text{K}^{-1}$ , respectively. Thereafter, the  $K$  of the composite PCMs increases slowly to  $5.62 \text{ Wm}^{-1}\text{K}^{-1}$  for 20 wt% EG loading. This is because the graphite flakes of EG are coated with a paraffin layer before the compression operation, causing a high interface thermal resistance between the EG flakes. With the increase of EG mass fraction, the paraffin layer becomes thinner, and the interface thermal resistance decreases. When the EG content reaches 15 wt%, the contact thermal resistance between the EG flakes becomes the critical factor to restrict heat transfer; therefore, the increase of  $K$  slows down. Detailed information on the thermal properties of the paraffin and composite PCMs is listed in Table 2.

**Table 2.** The thermal properties of paraffin and composite PCMs.

Sample	Melt		Solidification		Thermal Conductivity $K (\text{Wm}^{-1}\text{K}^{-1})$
	$T_m (\text{°C})$	$\Delta H_m (\text{J/g})$	$T_s (\text{°C})$	$\Delta H_s (\text{J/g})$	
Paraffin	42.79	205.20	36.22	203.89	0.21
PCM-1	43.46	192.14	36.80	191.79	2.09
PCM-2	43.04	172.06	34.96	170.97	3.85
PCM-3	42.42	157.81	34.34	154.96	5.39
PCM-4	42.88	144.08	33.55	140.71	5.62

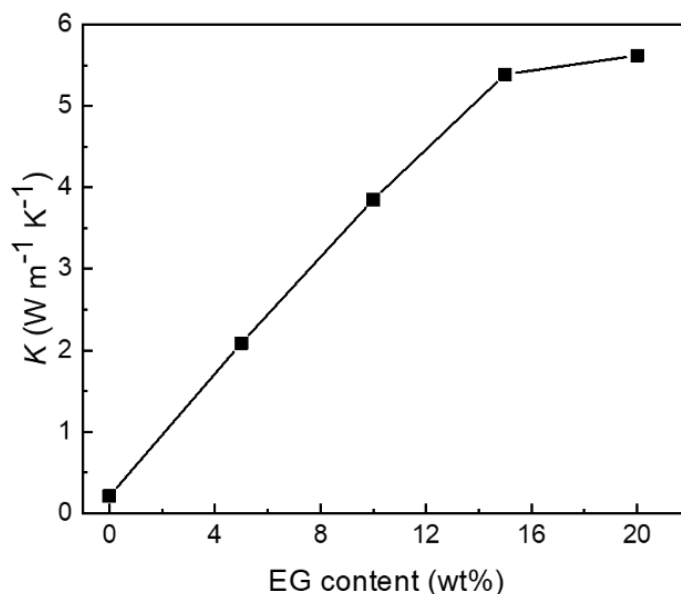


Figure 6. Thermal conductivity of paraffin and composite PCMs as a function of EG content.

Further, Figure 7 compares the thermal conductivity and melting enthalpy of our composites with other composite PCMs recently reported [31,36,39–43]; the information on other composite PCMs is detailed in Table 3. For the evaluation of composite PCMs, it is necessary to make a comprehensive comparison of enthalpy and thermal conductivity. It can be observed that the composite PCMs in this work are located in the upper right corner of the figure, which means that their performance outperforms that of other published results.

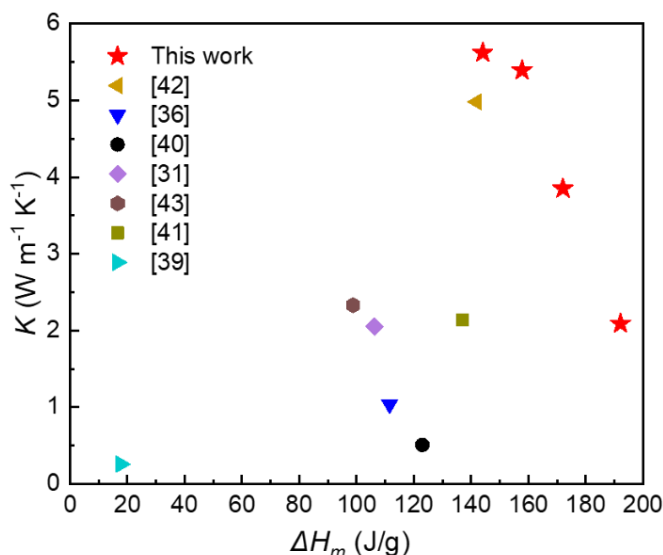


Figure 7. The comparison of thermal conductivity and melting enthalpy between our composite PCMs and other composite PCMs recently reported.

Thermal stability is also essential to ensure the long-term thermal storage capacity of composite PCMs. Figure 8 displays the TG curves of paraffin, LDPE, and composite PCMs. The paraffin begins to decompose at 150 °C, and LDPE at 380 °C. As for the composite PCMs, their degradation process is divided into two stages, corresponding to the decomposition of paraffin and LDPE, respectively. All of them have good thermal stability. Moreover, the residual mass fractions of the composite PCMs are 4.6%, 9.8%, 14.9%, and 19.8%, respectively, which is consistent with their EG mass fractions, indicating

good uniformity of the samples. It can be observed that the degradation temperature of the composite PCMs does not change, but their degradation rate is significantly faster than that of paraffin. This is because the presence of EG facilitates heat transfer through the composite PCMs.

**Table 3.** The summary of thermal conductivity and melting enthalpy of other composite PCMs recently reported.

Sample	$K$ ( $\text{Wm}^{-1}\text{K}^{-1}$ )	$\Delta H_m$ (J/g)	Ref
Tailing porous ceramics/paraffin	0.51	123	[40]
Copper foam/reduced graphene oxide /paraffin	1.04	111.53	[36]
Wood flour/high density polyethylene/EG/paraffin	0.258	17.79	[39]
Epoxy/EG/paraffin	4.98	142	[42]
Epoxy/EG/paraffin	2.141	137	[41]
Silica/EG/paraffin	2.053	106.2	[31]
EG/solid–solid PCM (polymer octadecyl acrylate)	2.33	98.8	[43]

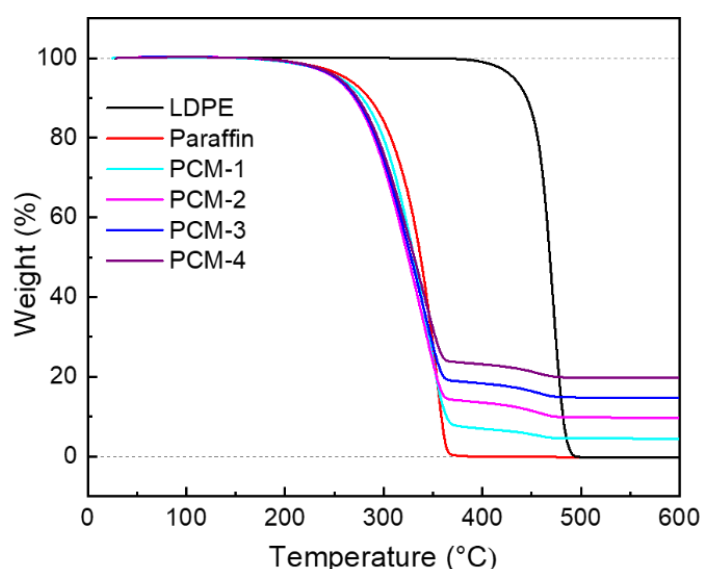


**Figure 8.** TG curves of paraffin, LDPE, and composite PCMs.

### 3.4. Weight Loss Ratios of the Composite PCMs

To improve the volumetric heat storage capacity for BTM, the composite PCMs must be compressed to increase their compactness [44]. However, a high level of compacting will impair the porosity of the EG matrix and squeeze the paraffin out of the EG matrix [45]. Figure 9 shows the weight loss ratios of composite PCMs versus the heating and cooling cycle numbers, and the data are calculated according to Equation (1). When the EG content is only 5 wt%, the weight loss ratio of the composite PCM rises sharply to 46.7% after 20 heating and cooling cycles without convergence, and the paraffin leakage is uncontrolled. However, when EG content reaches 10 wt%, 15 wt%, and 20 wt%, the weight loss ratios of the composite PCMs can stabilize at 6.2%, 4.3%, and 1.4%, respectively. To maintain the high heat storage capacity of composite PCMs during long-term service, it is essential to suppress paraffin leakage. Therefore, it is recommended to keep the mass fraction of EG in a composite PCM above 10%.

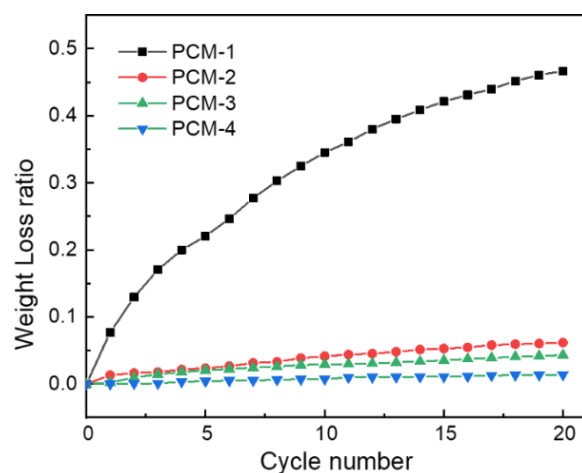


**Figure 9.** Weight loss ratios of composite PCMs versus cycle number of heating and cooling.

Figure 10a,b show the photographs of samples S-1 and PCM-2 after 20 heating and cooling cycles. Due to the thermal expansion of paraffin, the EG medium cracks. It can be observed that the surface of sample S-1 becomes extremely rough and cracked. As a result, the composite PCM cannot fit on the battery surface, and the thermal contact resistance between them increases, reducing the heat dissipation efficiency. With the addition of LDPE, the mechanical strength of the composite PCM is improved, and the polymer interpenetrating network shares the internal stress of paraffin expansion. It can be seen that the surface of the PCM-2 sample remains flat without deformation. This result shows that when the LDPE content reaches 40% of the EG mass, the composite PCM has the basic mechanical strength to resist the internal stress of paraffin expansion. To improve the paraffin mass fraction in composite PCMs and maintain high latent heat, LDPE should not be added further.

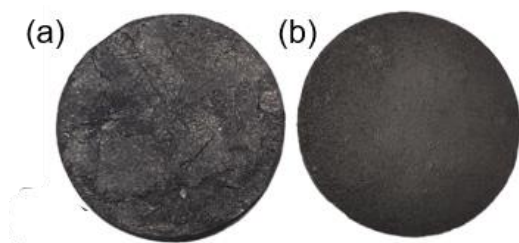


**Figure 10.** Photographs of (a) S-1 and (b) PCM-2 samples after 20 heating and cooling cycles.

### 3.5. Thermal Management Properties of the Composite PCMs

Figure 11 shows the temperature variations of the battery middle surface with and without composite PCMs. It confirms that air cooling is too inefficient to meet the heat dissipation requirements due to the low heat transfer coefficient. As the battery was not wrapped with the composite PCM when discharged, the temperature rose sharply from 25 °C to 46.6 °C. After wrapping with PCM-1, PCM-2, PCM-3, and PCM-4, the battery temperature drops to 41.4 °C, 34.7 °C, 38.8 °C, and 39.3 °C, respectively. Excellent thermal conductivity and high enthalpy are desirable for PCM materials applied in BTM. Among the composite PCMs, the cooling effect of PCM-1 is relatively poor. This may be because its thermal conductivity is not high enough to allow the heat to spread out in time. Evidently, due to concurrent great thermal conductivity ( $3.85 \text{ Wm}^{-1}\text{K}^{-1}$ ) and enthalpy ( $172.06 \text{ J/g}$ ), PCM-2 exhibits the best thermal management performance, reducing battery temperature rise by 55.1%. As for PCM-3 and PCM-4, the battery temperature variation shows a downward trend resulting from lower enthalpy.

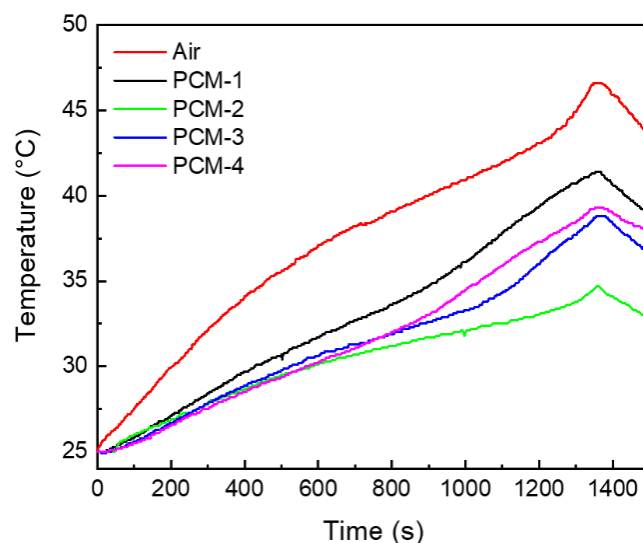


**Figure 11.** Temperature variations of battery surface with and without composite PCMs.

#### 4. Conclusions

In summary, a ternary composite PCM consisting of EG, paraffin, and LDPE was manufactured by physical blending and cold pressing. The EG can effectively encapsulate paraffin and improve the thermal conductivity of the composite PCM. The LDPE interpenetrating network can reinforce the mechanical strength of the composite PCM and resist the internal stress of paraffin expansion. When 10 wt% EG and 4 wt% LDPE were added, the enthalpy and thermal conductivity of composite PCM could reach 172.06 J/g and  $3.85 \text{ Wm}^{-1}\text{K}^{-1}$ , and its weight loss ratio could be under control and stabilized at 6.2%. Excellently, the composite PCM reduces the temperature rise of the battery by 55.1% and exhibits outstanding thermal management performance. In short, this work provides a simple and efficient route to fabricate a composite PCM to meet the requirement of battery thermal management.

**Author Contributions:** Methodology, S.W. and C.X.; validation, Y.Y. and H.Q.; formal analysis, Y.Y., H.Q. and S.R.; investigation, Y.Y. and J.S.; resources, Y.Y., J.S. and W.X.; data curation, Y.Y. and H.Q.; writing—original draft preparation, Y.Y. and H.Q.; writing—review and editing, S.W.; visualization, H.Q.; supervision, S.W. and C.X.; project administration, S.W.; funding acquisition, S.W. and C.X. All authors have read and agreed to the published version of the manuscript.

**Funding:** This research was funded by the Fundamental Research Funds for the Central Universities (WUT: 2019IVA003).

**Data Availability Statement:** Not applicable.

**Acknowledgments:** The authors gratefully thank the Fundamental Research Funds for the Central Universities (WUT: 2019IVA003).

**Conflicts of Interest:** The authors declare no conflict of interest.

#### References

1. Ibrahim, A.; Jiang, F.M. The electric vehicle energy management: An overview of the energy system and related modeling and simulation. *Renew. Sust. Energ. Rev.* **2021**, *144*, 111049. [[CrossRef](#)]
2. He, C.; Li, M.; Wang, F.; Zheng, J. Simulation study of a cylindrical battery module. *J. Energy Storage* **2022**, *48*, 104000. [[CrossRef](#)]
3. Li, J.; Huang, J.; Cao, M. Properties enhancement of phase-change materials via silica and Al honeycomb panels for the thermal management of LiFeO<sub>4</sub> batteries. *Appl. Therm. Eng.* **2018**, *131*, 660–668. [[CrossRef](#)]
4. Zichen, W.; Changqing, D. A comprehensive review on thermal management systems for power lithium-ion batteries. *Renew. Sustain. Energy Rev.* **2021**, *139*, 110685. [[CrossRef](#)]
5. Ramadass, P.; Haran, B.; White, R.; Popov, B.N. Capacity fade of Sony 18650 cells cycled at elevated temperatures. *J. Power Sources* **2002**, *112*, 614–620. [[CrossRef](#)]

6. Motloch, C.G.; Christophersen, J.P.; Belt, J.R.; Wright, R.B.; Hunt, G.L.; Sutula, R.A.; Duong, T.; Tartamella, T.J.; Haskins, H.J.; Miller, T.J. High-Power Battery Testing Procedures and Analytical Methodologies for HEVs. *SAE Trans.* **2002**, *111*, 797–802.
7. Landini, S.; Leworthy, J.; O'Donovan, T.S. A Review of Phase Change Materials for the Thermal Management and Isothermalisation of Lithium-Ion Cells. *J. Energy Storage* **2019**, *25*, 100887. [[CrossRef](#)]
8. Wei, Z.; Zhao, J.; Xiong, B. Dynamic electro-thermal modeling of all-vanadium redox flow battery with forced cooling strategies. *Appl. Energy* **2014**, *135*, 1–10. [[CrossRef](#)]
9. Wu, W.; Wang, S.; Wu, W.; Chen, K.; Hong, S.; Lai, Y. A critical review of battery thermal performance and liquid based battery thermal management. *Energy Convers. Manag.* **2019**, *182*, 262–281. [[CrossRef](#)]
10. Al-Hallaj, S.; Selman, J.R. Thermal modeling of secondary lithium batteries for electric vehicle/hybrid electric vehicle applications. *J. Power Sources* **2002**, *110*, 341–348. [[CrossRef](#)]
11. Sabbah, R.; Kizilel, R.; Selman, J.R.; Al-Hallaj, S. Active (air-cooled) vs. passive (phase change material) thermal management of high power lithium-ion packs: Limitation of temperature rise and uniformity of temperature distribution. *J. Power Sources* **2008**, *182*, 630–638. [[CrossRef](#)]
12. Tiskatine, R.; Aharoune, A.; Bouirden, L.; Ihlal, A. Identification of suitable storage materials for solar thermal power plant using selection methodology. *Appl. Therm. Eng.* **2017**, *117*, 591–608. [[CrossRef](#)]
13. Reddy, K.S.; Mudgal, V.; Mallick, T.K. Review of latent heat thermal energy storage for improved material stability and effective load management. *J. Energy Storage* **2018**, *15*, 205–227. [[CrossRef](#)]
14. Lazrak, A.; Fourmigué, J.-F.; Robin, J.-F. An innovative practical battery thermal management system based on phase change materials: Numerical and experimental investigations. *Appl. Therm. Eng.* **2018**, *128*, 20–32. [[CrossRef](#)]
15. Sharma, R.K.; Ganesan, P.; Tyagi, V.V.; Metselaar, H.S.C.; Sandaran, S.C. Developments in organic solid–liquid phase change materials and their applications in thermal energy storage. *Energy Convers. Manag.* **2015**, *95*, 193–228. [[CrossRef](#)]
16. Kahwaji, S.; White, M.A. Organic Phase Change Materials for Thermal Energy Storage: Influence of Molecular Structure on Properties. *Molecules* **2021**, *26*, 6635. [[CrossRef](#)] [[PubMed](#)]
17. Wang, J.; Hao, Y.; Zhu, B.; Han, T.; Li, Z.; Zhang, J. Crystalline Behavior of Paraffin Wax. *J. Phys. Chem. B* **2022**, *126*, 985–995. [[CrossRef](#)]
18. Chang, Z.; Wang, K.; Wu, X.; Lei, G.; Wang, Q.; Liu, H.; Wang, Y.; Zhang, Q. Review on the preparation and performance of paraffin-based phase change microcapsules for heat storage. *J. Energy Storage* **2022**, *46*, 103840. [[CrossRef](#)]
19. Umair, M.M.; Zhang, Y.; Iqbal, K.; Zhang, S.; Tang, B. Novel strategies and supporting materials applied to shape-stabilize organic phase change materials for thermal energy storage—A review. *Appl. Energy* **2019**, *235*, 846–873. [[CrossRef](#)]
20. Liu, L.; Su, D.; Tang, Y.; Fang, G. Thermal conductivity enhancement of phase change materials for thermal energy storage: A review. *Renew. Sustain. Energy Rev.* **2016**, *62*, 305–317. [[CrossRef](#)]
21. Mishra, D.K.; Bhowmik, C.; Bhowmik, S.; Pandey, K.M. Property-enhanced paraffin-based composite phase change material for thermal energy storage: A review. *Env. Sci. Pollut. Res. Int.* **2022**, *29*, 43556–43587. [[CrossRef](#)] [[PubMed](#)]
22. Lv, P.; Liu, C.; Rao, Z. Review on clay mineral-based form-stable phase change materials: Preparation, characterization and applications. *Renew. Sustain. Energy Rev.* **2017**, *68*, 707–726. [[CrossRef](#)]
23. Hamidi, E.; Ganesan, P.B.; Sharma, R.K.; Yong, K.W. Computational study of heat transfer enhancement using porous foams with phase change materials: A comparative review. *Renew. Sustain. Energy Rev.* **2023**, *176*, 113196. [[CrossRef](#)]
24. Li, M.; Mu, B. Effect of different dimensional carbon materials on the properties and application of phase change materials: A review. *Appl. Energy* **2019**, *242*, 695–715. [[CrossRef](#)]
25. Liu, Z.-X.; Jiang, L.-Y.; Wang, X.-X.; Ma, M.-J.; Lu, Q.-Q.; Liang, P. Novel expanded graphite with a ‘Spitball’ structure. *Mater. Sci. Technol.* **2021**, *38*, 1–4. [[CrossRef](#)]
26. Zhang, Z.; Fang, X. Study on paraffin/expanded graphite composite phase change thermal energy storage material. *Energy Convers. Manag.* **2006**, *47*, 303–310. [[CrossRef](#)]
27. Dong, Q.; Sun, B.; Dong, Z.; Tian, Y.; Zhu, H.; Yuan, G.; Cong, Y.; Li, B.; Guo, J.; Li, X. Construction of highly efficient heat conduction channels within expanded graphite/paraffin phase change composites and their thermophysical properties. *Energy Rep.* **2022**, *8*, 7071–7084. [[CrossRef](#)]
28. Lv, Y.; Yang, X.; Li, X.; Zhang, G.; Wang, Z.; Yang, C. Experimental study on a novel battery thermal management technology based on low density polyethylene-enhanced composite phase change materials coupled with low fins. *Appl. Energy* **2016**, *178*, 376–382. [[CrossRef](#)]
29. JianShe, H.; Chao, Y.; Xu, Z.; Jiao, Z.; JinXing, D. Structure and thermal properties of expanded graphite/paraffin composite phase change material. *Energy Sources Part A Recovery Util. Environ. Eff.* **2018**, *41*, 86–93. [[CrossRef](#)]
30. Drissi, S.; Ling, T.-C.; Mo, K.H. Thermal efficiency and durability performances of paraffinic phase change materials with enhanced thermal conductivity—A review. *Thermochim. Acta* **2019**, *673*, 198–210. [[CrossRef](#)]
31. Liu, S.; Fei, X.; Zhang, B.; Zhao, H.; Wan, M. Expanded graphite/paraffin/silica phase change composites with high thermal conductivity and low permeability prepared by the solid-state wet grinding method. *Sol. Energy Mater. Sol. Cells* **2022**, *236*, 111484. [[CrossRef](#)]
32. Liu, X.; Wang, C.; Wu, T.; Li, Z.; Wu, C. A novel stable and flexible composite phase change materials for battery thermal management. *Appl. Therm. Eng.* **2022**, *212*, 118510. [[CrossRef](#)]

33. Chriaa, I.; Karkri, M.; Trigui, A.; Jedidi, I.; Abdelmouleh, M.; Boudaya, C. The performances of expanded graphite on the phase change materials composites for thermal energy storage. *Polymer* **2021**, *212*, 123128. [[CrossRef](#)]
34. Liu, C.; Song, Y.; Xu, Z.; Zhao, J.; Rao, Z. Highly efficient thermal energy storage enabled by a hierarchical structured hyper-crosslinked polymer/expanded graphite composite. *Int. J. Heat Mass Transf.* **2020**, *148*, 119068. [[CrossRef](#)]
35. Wu, M.; Li, T.; He, Q.; Du, R.; Wang, R. Thermally conductive and form-stable phase change composite for building thermal management. *Energy* **2022**, *239*, 121938. [[CrossRef](#)]
36. Zhang, H.; Wang, L.; Xi, S.; Xie, H.; Yu, W. 3D porous copper foam-based shape-stabilized composite phase change materials for high photothermal conversion, thermal conductivity and storage. *Renew. Energy* **2021**, *175*, 307–317. [[CrossRef](#)]
37. Lu, B.; Zhang, Y.; Sun, D.; Jing, X. Experimental investigation on thermal properties of paraffin/expanded graphite composite material for low temperature thermal energy storage. *Renew. Energy* **2021**, *178*, 669–678. [[CrossRef](#)]
38. Cai, W.; Yang, W.; Jiang, Z.; He, F.; Zhang, K.; He, R.; Wu, J.; Fan, J. Numerical and experimental study of paraffin/expanded graphite phase change materials with an anisotropic model. *Sol. Energy Mater. Sol. Cells* **2019**, *194*, 111–120. [[CrossRef](#)]
39. Guo, X.; Zhang, S.; Cao, J. An energy-efficient composite by using expanded graphite stabilized paraffin as phase change material. *Compos. Part A Appl. Sci. Manuf.* **2018**, *107*, 83–93. [[CrossRef](#)]
40. Li, R.; Zhou, Y.; Duan, X. A novel composite phase change material with paraffin wax in tailings porous ceramics. *Appl. Therm. Eng.* **2019**, *151*, 115–123. [[CrossRef](#)]
41. Ren, X.; Shen, H.; Yang, Y.; Yang, J. Study on the properties of a novel shape-stable epoxy resin sealed expanded graphite/paraffin composite PCM and its application in buildings. *Phase Transit.* **2019**, *92*, 581–594. [[CrossRef](#)]
42. Tao, Z.; Wang, H.; Liu, J.; Zhao, W.; Liu, Z.; Guo, Q. Dual-level packaged phase change materials – thermal conductivity and mechanical properties. *Sol. Energy Mater. Sol. Cells* **2017**, *169*, 222–225. [[CrossRef](#)]
43. Xiao, C.; Zhang, G.; Li, Z.; Yang, X. Custom design of solid–solid phase change material with ultra-high thermal stability for battery thermal management. *J. Mater. Chem. A* **2020**, *8*, 14624–14633. [[CrossRef](#)]
44. Jiang, G.; Huang, J.; Fu, Y.; Cao, M.; Liu, M. Thermal optimization of composite phase change material/expanded graphite for Li-ion battery thermal management. *Appl. Therm. Eng.* **2016**, *108*, 1119–1125. [[CrossRef](#)]
45. Ling, Z.; Chen, J.; Fang, X.; Zhang, Z.; Xu, T.; Gao, X.; Wang, S. Experimental and numerical investigation of the application of phase change materials in a simulative power batteries thermal management system. *Appl. Energy* **2014**, *121*, 104–113. [[CrossRef](#)]

**Disclaimer/Publisher’s Note:** The statements, opinions and data contained in all publications are solely those of the individual author(s) and contributor(s) and not of MDPI and/or the editor(s). MDPI and/or the editor(s) disclaim responsibility for any injury to people or property resulting from any ideas, methods, instructions or products referred to in the content.